Received: 4 February 2021 | Revised: 22 February 2021 | Accepted: 27 February 2021

DOI: 10.1002/aoc.6233

FULL PAPER

Applied Organometallic Chemistry WILEY

Magnetite@MCM-41 nanoparticles as support material for Pd-*N*-heterocyclic carbene complex: A magnetically separable catalyst for Suzuki–Miyaura reaction

Mitat Akkoç[1] | **Nesrin Buğday**[2] | **Serdar Altın**[3] | **Sedat Yaşar**[2]

[1]Hekimhan Vocational College, Department of Property Protection and Security, Malatya Turgut Özal University, Malatya, Turkey

[2]Faculty of Science and Arts, Department of Chemistry, İnönü University, Malatya, Turkey

[3]Faculty of Science and Arts, Department of Physics, İnönü University, Malatya, Turkey

Correspondence

Sedat Yaşar, İnönü University, Faculty of Science and Arts, Department of Chemistry, 44280 Malatya, Turkey.
Email: sedat.yasar@inonu.edu.tr

Mitat Akkoç, Hekimhan Vocational College, Department of Property Protection and Security, Malatya Turgut Özal University, Hekimhan, Malatya, Turkey.
Email: mitat.akkoc@ozal.edu.tr

The Magnetite@MCM-41@NHC@Pd catalyst was obtained with Pd metal bound to the NHC ligand anchored to the surface of Fe_3O_4@MCM-41. It was characterized by Fourier transform infrared (FTIR) spectroscopy, transmission electron microscopy (TEM), X-ray diffraction (XRD), X-ray photoelectron spectroscopy (XPS), energy disperse X-ray analysis (EDX), thermogravimetric analysis (TGA), differential thermal analysis (DTA), and scanning electron microscopy (SEM). The amount of Pd in the Magnetite@MCM-41@NHC@Pd was measure by inductively coupled plasma–optical emission spectroscopy (ICP-OES) analysis. The catalytic activity of Magnetite@MCM-41@NHC@Pd heterogeneous catalyst done on Suzuki–Miyaura reactions of aryl halides with different substituted arylboronic acid derivatives. All coupling reactions afforded excellent yields and up to 408404 Turnover Frequency (TOF) h^{-1} in the presence of 2 mg of Magnetite@MCM-41@NHC@Pd catalyst (0.0564 mmol g^{-1}, 0.01127 mmol% Pd) at room temperature in 2-propanol/H_2O (1:2). Moreover, Magnetite@MCM-41@NHC@Pd catalyst was recover by applying the magnet and reused for another reaction. The catalyst showed excellent structural and chemical stability and reused ten times without a substantial loss in its catalytic performance.

KEYWORDS

magnetic palladium catalyst, magnetite, MCM-41, Pd (II)-*N*-heterocyclic carbene, Suzuki–Miyaura reaction

1 | INTRODUCTION

Supported materials have attracted considerable attention in recent years. The materials have many uses in fields such as chemistry, medicine, and biological sciences.[1–7] In the last two decades, the use of these materials increased rapidly. Therefore, the design and preparation of the heterogeneous catalyst are crucial. Immobilization of heterogeneous catalysts with homogeneous species is an essential method for fabricating new types of supported catalysts.[8–13]

Magnetic nanoparticles (MNPs) and mesoporous materials have attracted significant attention due to their outstanding features in the context of green chemistry. The application of MNPs in catalysis increases has gained great attention. Because MNPs are superparamagnetic, have low toxicity, show biocompatibility, and have high magnetic susceptibility,[14–20] MNPs are used either support materials or active components in catalysis due to their chemical activity, robustness, and reusability. Besides these superior properties of MNPs, they have disadvantages such as low surface area and poor

https://doi.org/10.1002/aoc.6233

durability. To overcome such disadvantages, the MNPs doped with mesoporous materials such as SiO_2, Santa Barbara Amorphous (SBA-15), and Mobil Composition of Matter (MCM-41). Mesoporous materials offer a high surface area, large and uniform pore volume, high temperature, and chemical stability.[21–24] The MCM-41 has more superior properties such as considerable durability, high specific surface area, air tolerance, large and uniform pore size, and high thermal and mechanical stability when compared to other mesoporous materials such as SiO_2, Santa Barbara Amorphous (SBA-15).[21–24] The Fe_3O_4 coated mesoporous materials offer superior advantages. It includes functionalization and preparation, air stability, non-toxicity, and incredibly facile separation from the reaction media by applied an external magnet.[25–32] Due to the large surface area of Fe_3O_4/MCM-41, the magnetite (Fe_3O_4) is introduced into the mesopores channels of MCM-41 to generate an ideal and excellent support for catalysts on catalytic applications.[33,34] Herein, to benefit from the superior features of MCM-41 mentioned above, we preferred MCM-41 mesoporous material for coated MNPs instead of SBA-15 and SiO_2.

N-heterocyclic carbenes (NHCs) are an excellent alternative to phosphine ligands because of their superior features. Thanks to its properties, such as ease to obtain, stability against air and moisture, and non-toxicity. The NHC ligands have better applications in homogeneous and heterogeneous catalysis. In order to synthesize the stable catalyst, the ligand has strong sigma donor property that led to the formation strong Metal-NHC bond.[35,36] This feature led to increasing the stability of the catalyst in different catalytic systems. Combining Pd-NHC with Fe_3O_4@MCM-41 is vital for synthesizing new types of MNPs catalysts for the organic transformation reactions. To date, several Pd-doped MNPs were successfully synthesized and used as the catalyst for C–C bond formation reactions.[34,37–53] The C–C bond formation reaction is a critical synthesis procedure in synthesizing natural products, agrochemicals, biologically active compounds, and pharmaceuticals.[33,34,38,44,48,50,54–56]

Although structurally similar catalysts exist in the literature, Pd complex of NHC ligand attached to the supporting material via the OH-group is not available in the literature. We synthesized this type of catalyst with the intelligent guess that such type catalyst maybe leads to high catalytic activity on the Suzuki–Miyaura reactions. Herein, we reported the fabrication and characterization of Fe_3O_4@MCM-41@NHC@Pd catalyst and investigation of catalytic activity on Suzuki–Miyaura reaction for a wide range of aryl bromides with different PhB $(OH)_2$ in aqueous media at room temperature.

2 | EXPERIMENTAL SECTION

2.1 | Materials and methods

Otherwise stated, all manipulations carried out in aerobic conditions. All chemicals purchased *Sigma Aldrich* or *Fluorochem* or *BLDpharm* companies and used as obtained. For NMR analysis, a Bruker Avance III 400-MHz Nuclear magnetic resonance (NMR) spectrometer was used at room temperature with the decoupled nucleus, using $CDCl_3$ and DMSO-d_6 as the solvent referenced versus Tetramethylsilane (TMS) as standard. All reactions were monitored on a Shimadzu GC2010 Plus system by gas chromatography–flame ionization detector (GC–FID) with an HP-5 column. Some of the catalytic products reported previously. The new catalytic products are characterized by different spectroscopic techniques. The GC–mass chromatography (MS) analysis of compounds was measured by Shimadzu GC–MS 2010 plus using a TRX-5 column on positive Electron Sprey Ionization (ESI) mode. The Fourier transform infrared (FTIR) analysis was performed with a PerkinElmer Spectrum 100 GladiATR FTIR spectrometer. An X-ray diffractometer performed the crystal structure analysis of the synthesized powder labeled Rigaku Rint 2000, powered by Cu K_α radiation for characterization. The scan rate chose as 2° min^{-1} between 2° and 80° min^{-1}. The microstructural properties and the synthesized powders' surface morphology investigated by Leo EVO-40 VPX scanning electron microscope (SEM). For X-ray **p**hotoelectron **s**pectroscopy (XPS) analyses: XPS instrument: PHI 5000 VersaProbe II, X rays: hn = 1486,6 eV monochromatic, spot 200 μm and Energy resolution (hi-resolution spectra): 0.8 eV were used. The transmission electron microscopy (TEM) analyses performed by FEI TECNAI OSIRIS operating at 200 kV, morphological analysis with HAADF-STEM imaging mode, chemical analysis with the Super-X energy disperse X-ray analysis (EDX) detector system (4 silicon drift detectors [SDDs]).

2.1.1 | General procedure for Suzuki–Miyaura reaction

Palladium nano-catalyst (2 mg, 0.01127 mmol%Pd), arylboronic acid (1.2 mmol), aryl halide (1 mmol), and K_2CO_3 (2 mmol) placed in a reaction tube under air and 3 ml of aqueous solution (2-propanol/water mixture [1:2, v:v]) were added to reaction tube and stirred at room temperature. The Fe_3O_4@MCM-41@NHC@Pd catalyst was removed by an external magnet from reaction media, and then 3 ml of H_2O and 3 ml of Et_2O

was added to the solution. The organic phase was separated and dried over $MgSO_4$. Filtrate was evaporated under reduced pressure to obtain the crude product. Some of the compounds were purified by column chromatography (Ethyl acetate/hexane as the eluent [1:30, v/v]). ^1H and ^{13}C NMR spectra of the new compounds (4-Methoxy-4′-nitro-3′-(trifluoromethyl)-[1,1′-biphenyl]-3-carbaldehyde and 4′-(tert-Butyl)-4-nitro-3-(trifluoromethyl)-1,1′-biphenyl) are presented in supporting information section (Figures S1 and S2, respectively).

2.2 | Synthesis

2.2.1 | Synthesis of NHC salt (1-(2,3,4,5,6-pentamethylbenzyl)-3-(ethanol)-benzimidazolium iodine)

The following procedure was used for the synthesis of NHC salt.[57] 2-Iodoethanole (1,8 g; 110 mmol) was added to 10 ml n-BuOH solution of 1-(2,3,4,5,6-pentamethylbenzyl)benzimidazole (2.78 g; 100 mmol). Then, the reaction solution refluxed for 4 h. After the reaction

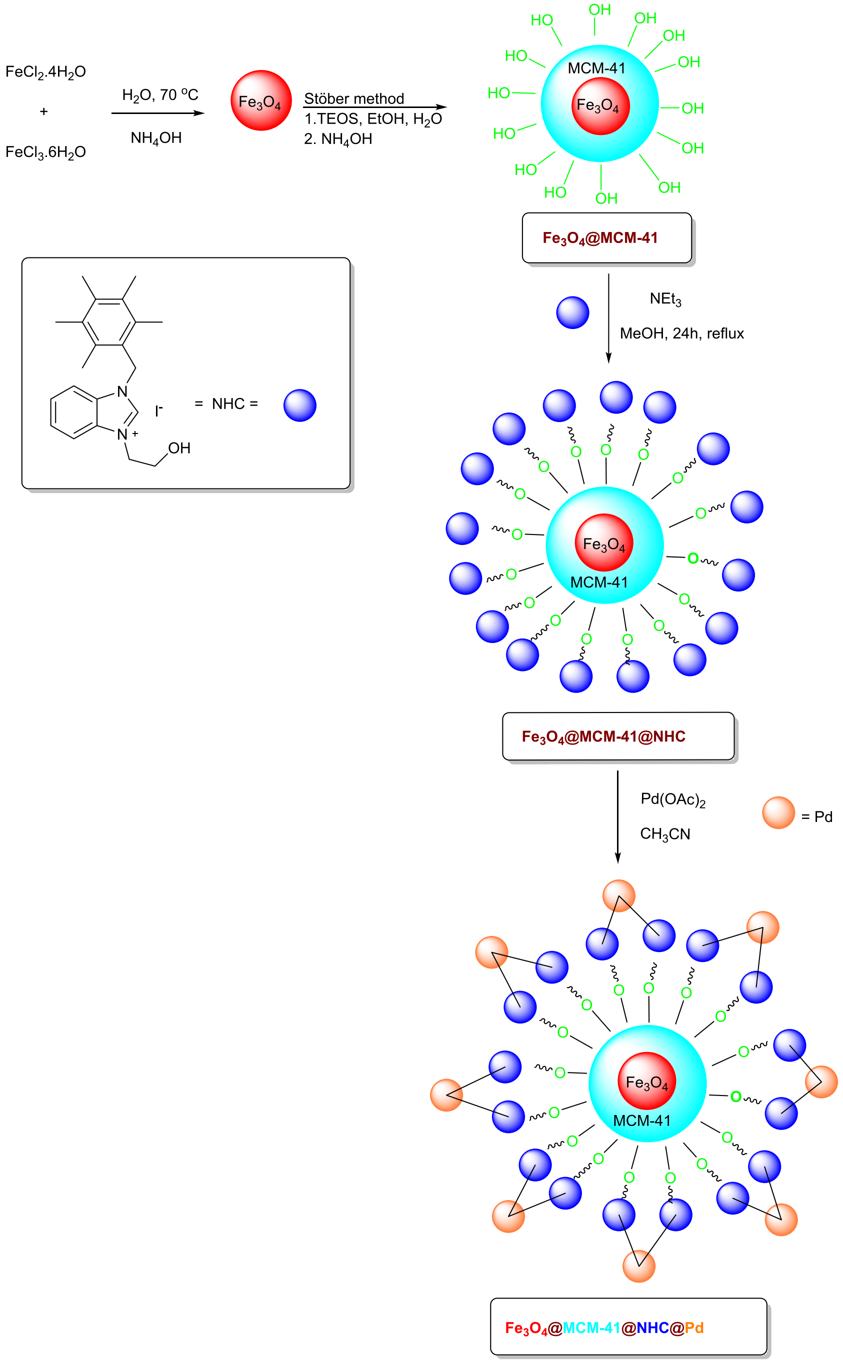

SCHEME 1 Synthesis pathway of the Magnetite@MCM-41@NHC-Pd catalyst

cooled to room temperature, yellow crystals form by themselves. Crystals were removed from the solution by filtration, washed with diethyl ether (5 × 5 ml), and dried by high vacuum. Yellow crystals were characterized by ^1H NMR, ^{13}C NMR, and elemental analysis. The ^1H and ^{13}C NMR spectra are presented in supporting information section (Figure S3).

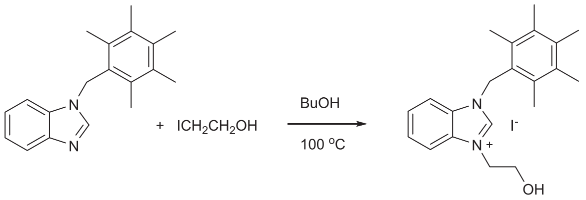

Yield: 75%, ^1H NMR (400 MHz, DMSO-d_6) δ = 8.97 (*s*, 1H, NC**H**N), 8.19 and 8.12 (*d*, *J* = 28 Hz, 4H, $C_6\mathbf{H_4}$), 5.72 (*s*, 2H, $\mathbf{CH_2}C_6[CH_3]_5$–2,3,4,5,6), 5.02 (*s*, 1H, $CH_2CH_2O\mathbf{H}$), 4.54 (*t*, *j* = 4.6 Hz, 2H, $CH_2\mathbf{CH_2}OH$), 3.74 (*m*, 2H, $\mathbf{CH_2}CH_2OH$), 2.27 (*s*, 3H, $CH_2C_6[\mathbf{CH_3}]_5$–2,3,**4**,5,6), 2.24 (*s*, 6H, $CH_2C_6[\mathbf{CH_3}]_5$–2,**3**,4,**5**,6), 2.21 (*s*, 6H, $CH_2C_6[\mathbf{CH_3}]_5$–**2**,3,4,5,**6**).^{13}C NMR (100 MHz, DMSO-d_6) δ = 141.8, 137.8, 134.4, 133.4, 132.1, 131.9, 127.1, 127.0, 125.9, 114.6, 114.3, 59.1, 49.8, 46.8, 17.5, 17.2, 16.9. Elemental analysis for $C_{21}H_{27}N_2OI$: %Calc. C:56.01, H:6.04, N:6.22; %found C:56.12, H:6.14, N:6.38.

2.2.2 | Catalyst preparation

The synthesis of the Fe_3O_4@MCM-41@NHC@Pd catalyst summarize in Scheme 1. The MNPs magnetite was synthesized via the coprecipitation method as previously reported with modifications using $FeCl_3.6H_2O$ and $FeCl_2.4H_2O$.[58] Synthesized Fe_3O_4 nanoparticles were coated with silica by tetraethylorthosilicate (TEOS) then doped in MCM-41 template to fabricate Fe_3O_4@MCM-41.[59] At the next step, Fe_3O_4@MCM-41 nanoparticles modified via the hydroxyl group on the NHC ligand. In the final step, Pd^{2+} was introduced to Fe_3O_4@MCM-41@NHC to afford Fe_3O_4@MCM-41@NHC@Pd catalyst labeled as **3** (Scheme 1). These Pd-doped nanoparticles characterize by TEM, SEM, FTIR, X-ray diffraction (XRD), XPS, differential thermal analysis (DTA), thermogravimetric analysis (TGA), and N_2 adsorption–desorption isotherms inductively coupled plasma–optical emission spectroscopy (ICP-OES) techniques. As a result of the ICP-OES analysis, it determined that the catalyst contains 0.6 wt% Pd (0.0564 mmol g^{-1}).

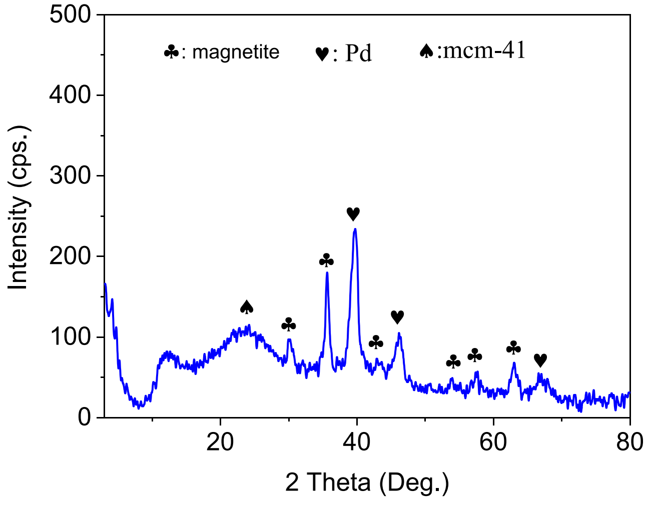

FIGURE 1 X-ray diffraction (XRD) pattern of magnetite@MCM-41@NHC-Pd

3 | RESULT AND DISCUSSIONS

3.1 | Catalyst characterization

The XRD pattern of Magnetite@MCM-41@NHC-Pd is given in Figure 1, and it is observed the reflection lines of magnetite, Pd, and MCM-41. There are no reactions between the components of the main structure. The magnetite is the center of the molecule, the MCM-41 was coated on magnetite, and NHC-Pd was dispersed on the MCM-41. The 2θ values at 30.18°, 35.6°, 42.92°, 54.94 °, 57.6°, and 63.13° belong to magnetite crystal planes, and 23.8° value is related to silica skeleton (JCPDF number: 19–0629). These 2θ values show the same pattern as the standard XRD pattern of magnetite and MCM-41.[33] Also, 2θ values at 39.67° (200), 46.19° (220), and 66.8° (331) in the XRD pattern belong to Pd^0 metal in the catalyst (JCPDF number: 46–1043). According to the results, it was observed that the target catalyst successfully synthesizes, and the results were compatible with the literature.[33]

The FTIR spectra for NHC, Magnetite@MCM-41, Magnetite@MCM-41@NHC, and magnetite@MCM-41@NHC-Pd are given in Figure 2. The peak at 584 cm^{-1} belongs to Fe–O bonds vibration,[27,60] and the band at 3421 cm^{-1} was associated with the O–H groups in the powders. The absorption bands at 1091, 799, and 464 cm^{-1} were attributed to Si–O–Si antisymmetric stretching vibrations, Si–O–Si symmetric stretching, and Si–O–Si or O–Si–O in MCM-41, respectively.[22,61] According to the FTIR results of Magnetite@MCM-41, Magnetite@MCM-41was successfully synthesized, and the results were compatible with the literature.

The FTIR band at 3506 cm^{-1} belongs to the OH group's symmetrical and asymmetrical stretching

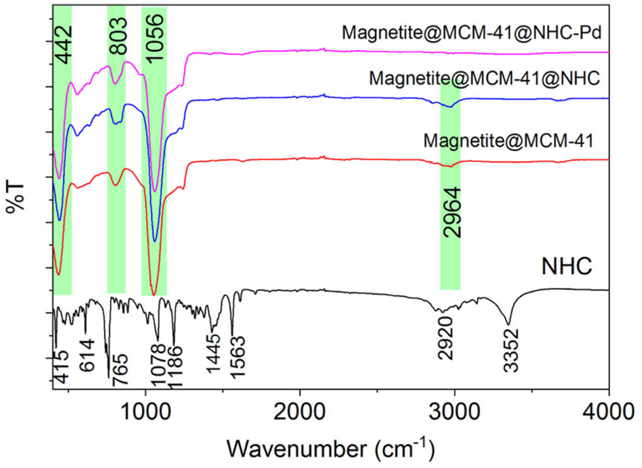

FIGURE 2 Fourier transform infrared (FTIR) spectra of NHC, Magnetite@MCM-41, Magnetite@MCM-41@NHC, and Magnetite@MCM-41@NHC-Pd

vibrations on the MCM-41.[62,63] The 2970 cm^{-1} (CH (C_bH_2) stretching, 2937 [CH (CH_2–CH_2) stretching], and 1600, 1400, 1300 cm^{-1} belong to NHC ligand. The characteristic spectral for NHC is the intense peak at 3352 cm^{-1} due to the supposition of the OH bending vibration. After immobilization of NHC to Magnetite@MCM-41 and Magnetite@MCM-41@NHC@Pd, the band at 3352 cm^{-1} disappeared, which indicates functionalization of Fe_3O_4@MCM-41 with NHC. The shift of absorption band at 1563 cm^{-1} (CNC stretching of benzimidazole) to 1394 cm^{-1} may be related to the formation of Pd–C bond (Pd-CNC stretching of benzimidazole) after reaction with Pd $(OAc)_2$.

The particle size, morphology, and the elemental distribution of Magnetite@MCM-41@NHC-Pd were studied by SEM and EDX techniques and shown in Figure 3. It was observed the spherical grain formations with uniform distribution as seen in the SEM mapping image. Furthermore, SEM images approve the nano-sized particle formation in the structure. The elemental distribution of the Magnetite@MCM-41@NHC-Pd was determined by EDX analysis and approved the existence of C, Si, O, N, Fe, and Pd atoms in the Magnetite @MCM-41@NHC@Pd catalyst with homogeneous distribution (Figure 3).

The elemental distribution of catalyst was also determined by HAADF–STEM analysis as presented in Figure 4. According to Figure 4, the elements are distributed homogeneously in the structure. Homogeneously dispersed Pd nanoparticles in the designed catalyst are desirable in the synthesis of heterogeneous catalysts. Although TEM analysis confirms that the sizes of Pd particles are between 80 and 95 nm (Figure 4), the particle size distribution should be calculated in detailed analysis. For this purpose, the particle size distribution was calculated by ImageJ open source program using SEM images and given in Figure 5. An area of 10 μm × 10 μm was used to calculate the distribution of particle size. According to the calculations, the catalyst particle size is between 200 nm and 1.2 μm, and the average particle size value was calculated as 650 (±180) nm. So, it concludes that nano-sized particles have characteristic structures with a high surface area for Magnetite@MCM-41@NHC-Pd catalyst which is important for catalytic reactions.

The XPS spectra of Magnetite@MCM-41@NHC-Pd and the detailed XPS spectra for each ion are presented

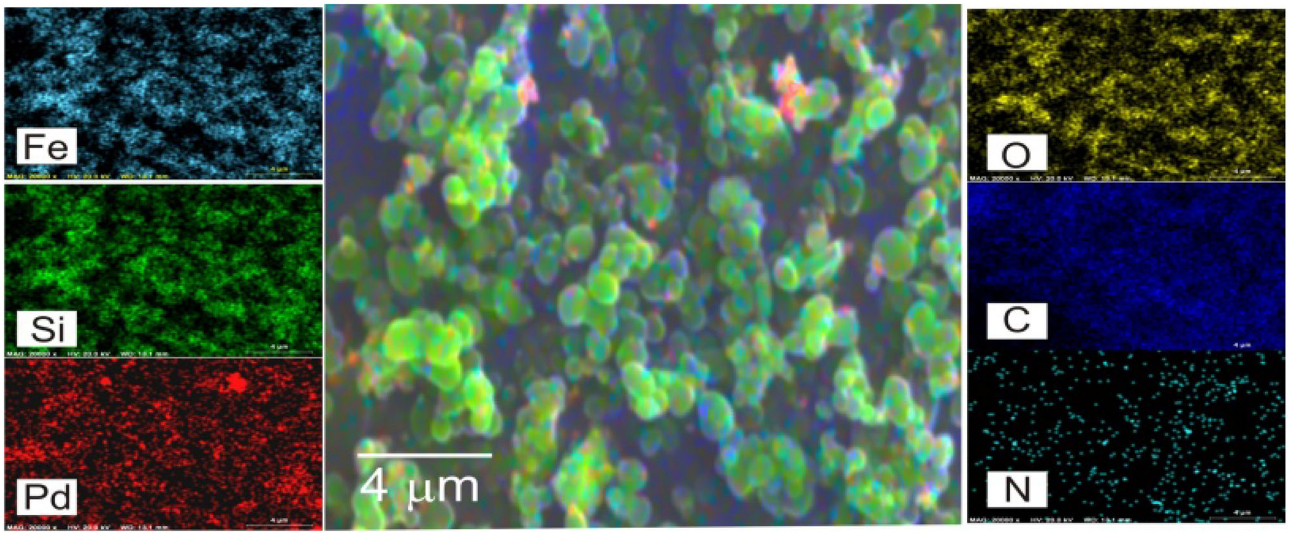

FIGURE 3 Scanning electron microscopy (SEM) and energy disperse X-ray analysis (EDX) dot mapping of Magnetite@MCM-41@NHC-Pd

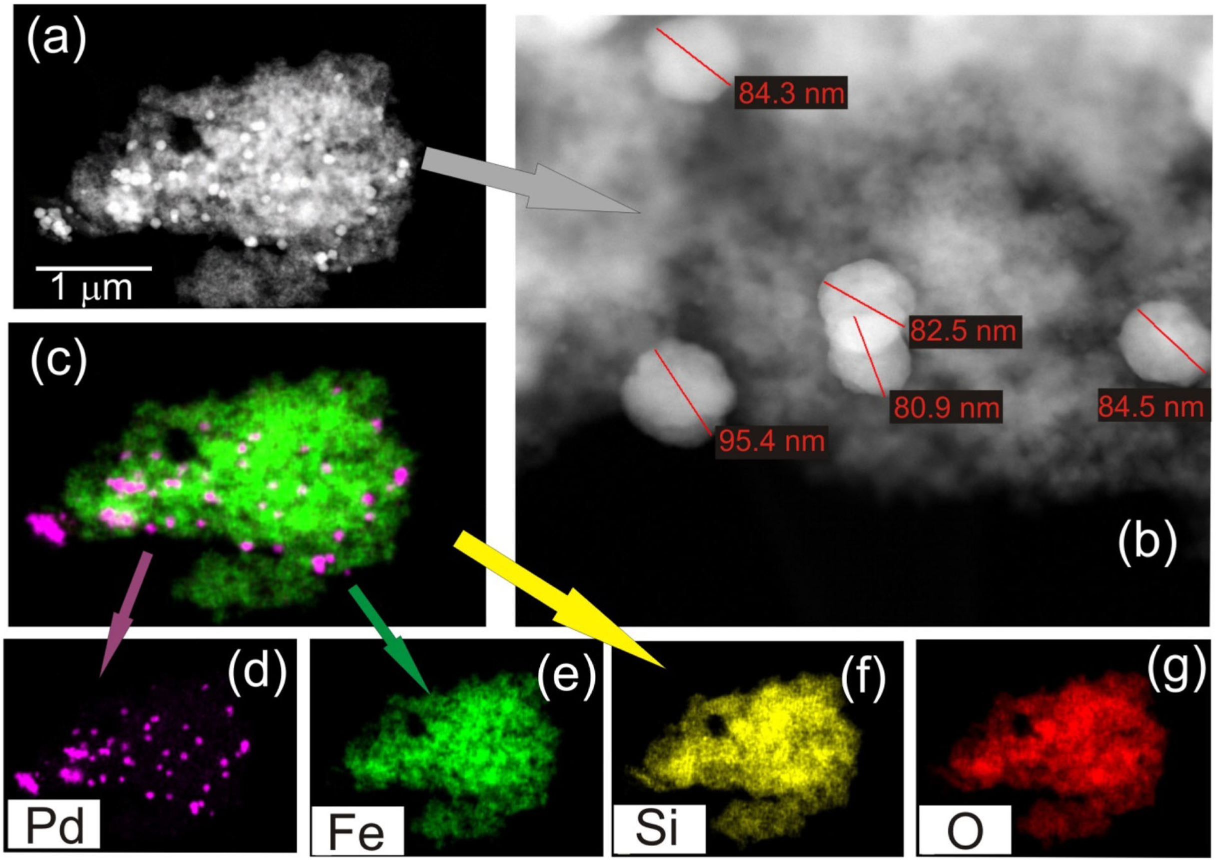

FIGURE 4 Transmission electron microscopy (TEM) images of Magnetite@MCM-41@NHC-Pd (a and b), energy disperse X-ray analysis (EDX)-dot mapping (c), and elemental distribution of Pd, Fe, Si, and O (d–g)

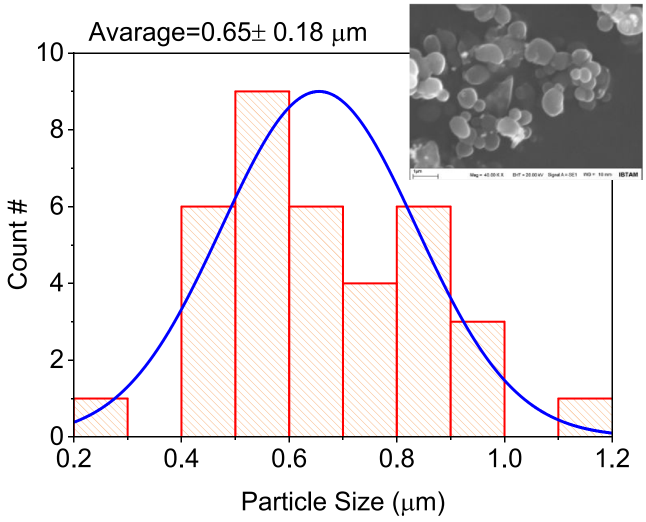

FIGURE 5 The particle size distribution of Magnetite@MCM-41@NHC-Pd

in Figure 6a–g. The XPS spectrum gives information about the aspect of all layers in the Magnetite@MCM-41@NHC-Pd. The XPS peaks of Magnetite@MCM-41@NHC-Pd given in Figure 6a confirm the presence of Si, C, O, N, Fe, and Pd^{2+} and Pd^{0} atoms. To learn more detail about each component in Figure 6a, we focused on each element in the powders shown in Figure 6b–g.

The energy level of C1s electrons observed at 285 eV, in Figure 6b and should be related to C–C/C=C bonds in the structure.[64] The N1s electron peak at 398 eV in Figure 6c is due to the imidazolate-N atom in the structure.[65] The peak at 531 eV for O1s belongs to the O atom in the NHC ligand, which has a −1 oxidation state (Figure 6d). The energy values of Si2s and Si2p electrons were observed at 152 and 102 eV, respectively, shown in Figure 6e,f. It is known that Fe3p represents the existence of Fe ions and Fe2p split into two energy levels at ~708 eV for 2p1/2 and ~721 eV for 2p3/2 (Figure 6g), and it explains by the formation of Fe^{2+} and Fe^{3+} in the structure of magnetite.[66] Figure 6h exhibits the XPS Pd 3d spectrum of catalyst reveals that Pd^{0} and Pd^{2+} oxidation states were observed. We attribute the binding energies of 332.84 and 338.17 eV for Pd^{0} 3d$_{5/2}$ and 3d$_{3/2}$ levels and the binding energies of 334.77 and 339.96 eV to Pd^{II} 3d$_{5/2}$ and 3d$_{3/2}$.[67] The Pd^{II} 3d$_{5/2}$ peak of Pd (OAc)$_2$ shifted from 338.7 to 334.77 eV, which verifies the synthesis of Pd (II)-NHC complex (Figure 6h). We can

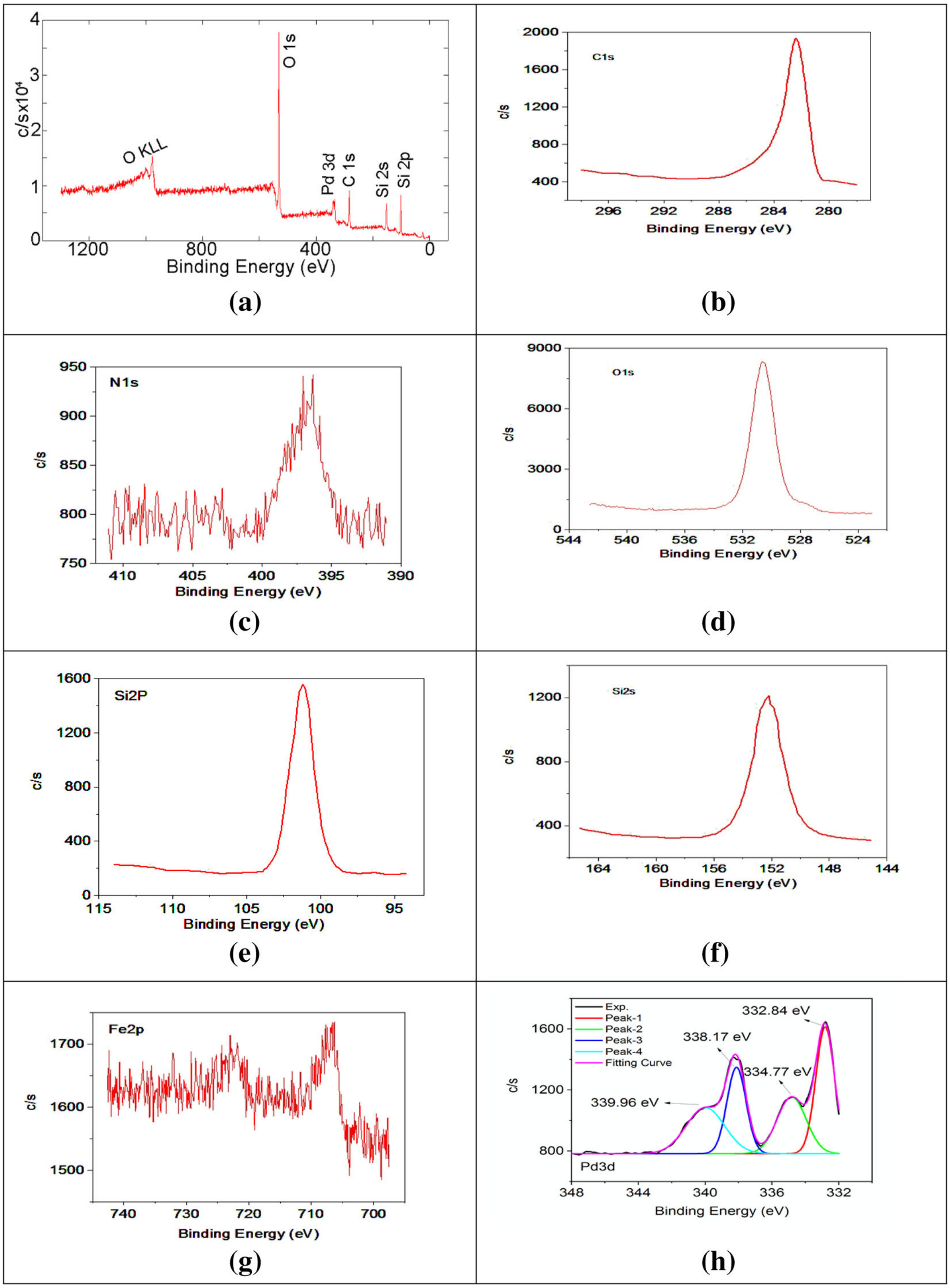

FIGURE 6 X-ray photoelectron spectroscopy (XPS) spectra of Magnetite@MCM-41@NHC@Pd (a), C1s (b), N1s (c), O1s (d), Si2p (e), Si2s (f), Fe2p (g), and Pd3d (h)

explain the presence of both Pd^0 and Pd^{2+} in the catalyst structure by the heating process during the synthesis of the catalyst, which reduces metals.[68] Although not all of Pd^{2+} reduced into Pd^0, the formation of any Pd^0 spices is the desired situation without using an extra agent. As a result, the XPS data show the presence of the atoms mentioned in the structure of the synthesized catalyst.[69]

The net amount of palladium doped into the structure of the catalyst was determined by ICP-OES analysis. According to the result, 0.6 wt% Pd (0.0564 mmol g^{-1}) was measured in the structure of Magnetite@MCM-41@NHC@Pd.

TGA was used for the determination of organic groups, which were immobilized on the surface of

Magnetite@MCM-41. The thermal stability of the Magnetite@MCM-41@NHC@Pd catalyst was evaluated by TGA and DTA as presented in Figure 7. DTA and TGA show that there are three regions for both data related to endothermic activity in the samples. The mass loss in low temperatures corresponds to the removed water and solvents.[70] The second weight loss at 234°C is related to the calcination of organic groups on the catalyst. The other two reactions at high temperatures are related to a thermal transformation of the crystal phase to the new stage, losing some oxygen and nitrogen ions from the structure, and condensation of the silanol groups of MCM-41.[22,33] So the Magnetite@MCM-41@NHC@Pd phase has stability without any decomposition up to 234°C which can be used for catalytic reactions in this temperature range.

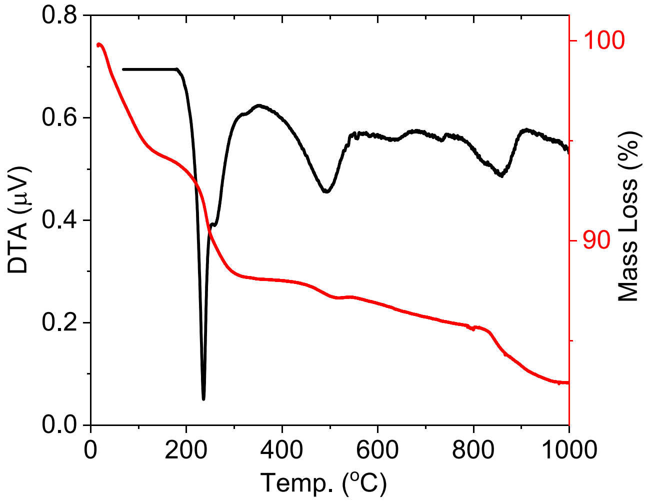

FIGURE 7 Differential thermal analysis (DTA) and thermogravimetric analysis (TGA) curve of Magnetite@MCM-41@NHC-Pd catalyst

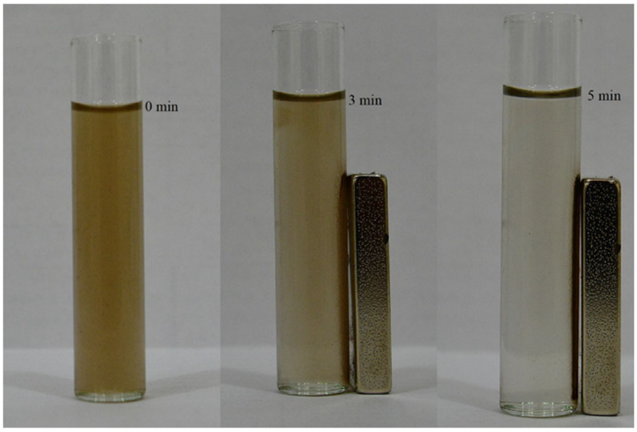

FIGURE 8 Magnetization of the Magnetite@MCM-41@NHC@Pd catalyst in the *i*-PrOH

Magnetite@MCM-41@NHC@Pd catalyst has high magnetization in the solvent. Figure 8 shows the tube containing the catalyst with an Nd magnet, which the catalyst in the solution accumulates near the magnet in a short time.

3.1.1 | Catalytic studies

We examine the catalytic activity of **3** for the Suzuki–Miyaura coupling reaction. The optimum reaction conditions for the Suzuki–Miyaura coupling reaction examine in a model reaction with bromoacetophenone and PhB(OH)$_2$, and the results are given in Table 1. Our previous studies[71–73] showed that the 2-propanol/H_2O solvent system and K_2CO_3 base are well compatible at room temperature in the homogeneous catalyze systems. Therefore, to determine the sufficient amount of catalyst directly, different reaction conditions are tested. To find an adequate amount of catalyst and reaction time, different catalyst loading at room temperature tested as shown in Table 1, Entries 1–5. When 2 mg of catalyst was used, the reaction was completed simultaneously with the same yield of 4 mg of the catalyst used (Table 1, Entries 1 and 3). However, the catalyst loading was reduced to 1 and 0.5 mg, reaction time increasing, and the product obtained in lower yield (Table 1, Entries 2 and 4). Thus, the sufficient amount of catalyst was determined to be 2 mg (0.01127 mmol% Pd). Also, the model reaction did not give any product when no catalyst was used (Table 1, Entry 5). After optimized catalyst loading and reaction temperature, different bases used model reaction. The K_2CO_3 base seems an appropriate base due to the high solubility feature in water (Table 1, Entries 6–10). When it comes to choosing the proper solvent for the catalytic system, the solvents such as 2-propanol, EtOH, water, dimethylformamide (DMF), and dioxane did not give good results due to insolubility or low solubility of 4-bromoacetophenone and PhB (OH)$_2$ in the same solvent (Table 1, Entries 11–18). The polar solvents mixture such as 2-propanol/H_2O mixture (1:2, v/v) creates the best solvent environment for the catalyst to give high efficiency. This solvent mixture causes good solubility in both substrates in the same environment. This aqueous mixture stands out as the best solvent for the reaction since they mix well with each other. 4-chloroacetophenone also tried to show the efficiency of catalyst on aryl chloride substrate. Unfortunately, no product formed in the reaction of 4-chloroacetophenone under the same reaction condition settled for aryl bromides (Table 1, Entry 19). However, an average yield was obtained in the reaction performed at 80°C for 12 h (Table 1, Entry 20). From these results, the

TABLE 1 Optimization of the conditions of phenylboronic acid and 4-bromoacetophenone catalyzed by **3**

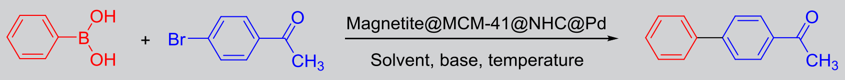

Entry	Catalyst loading	Base	Solvent	Temp./time	[a]Yield %
1	2 mg	K_2CO_3	H_2O/*i*-PrOH	rt, 0.5 min	100
2	1 mg	K_2CO_3	H_2O/*i*-PrOH	rt, 0.5 min	56
3	4 mg	K_2CO_3	H_2O/*i*-PrOH	rt, 0.5 min	100
4	0.5 mg	K_2CO_3	H_2O/*i*-PrOH	rt, 0.5 min	15
5	-	K_2CO_3	H_2O/*i*-PrOH	rt, 0.5 min	0
6	2 mg	NaOH	H_2O/*i*-PrOH	rt, 0.5 min	75
7	2 mg	Na_2CO_3	H_2O/*i*-PrOH	rt, 0.5 min	66
8	2 mg	Cs_2CO_3	H_2O/*i*-PrOH	rt, 0.5 min	58
9	2 mg	K^tOBu	H_2O/*i*-PrOH	rt, 0.5 min	40
10	2 mg	KOH	H_2O/*i*-PrOH	rt, 0.5 min	33
11	2 mg	K_2CO_3	H_2O	rt, 0.5 min	3
12	2 mg	K_2CO_3	*i*-PrOH	rt, 0.5 min	8
13	2 mg	K_2CO_3	EtOH	rt, 0.5 min	5
14	2 mg	K_2CO_3	DMF	rt, 0.5 min	12
15	2 mg	K_2CO_3	Dioxane	rt, 0.5 min	6
16	2 mg	K_2CO_3	DMF/H_2O	rt, 0.5 min	68
17	2 mg	K_2CO_3	H_2O/EtOH	rt, 0.5 min	92
18	2 mg	K_2CO_3	H_2O/Dioxane	rt, 0.5 min	56
19	2 mg	K_2CO_3	H_2O/*i*-PrOH	rt, 12 h	2
20	2 mg	K_2CO_3	H_2O/*i*-PrOH	80°C, 12 h	80

[a]Reaction conditions: Magnetite@MCM-41@NHC@Pd (2 mg, 0.01127 mmol%Pd), phenylboronic acid (0.6 mmol), 4-bromoacetophenone (0.5 mmol), base (1.0 mmol), and solvent (3 ml). Gas chromatography (GC) yields determine according to 4-bromoacetophenone using (trifluoromethyl)benzene as an internal standard.

developed catalytic system here is more suitable for cross-coupling reactions of aryl bromides than aryl chlorides. As a result of the reactions tested with different parameters, the optimum reaction condition determined as follows: 2 mg (0.01127 mmol% Pd) of catalyst, 0.5-mmol ArBr, 0.6-mmol PhB $(OH)_2$, 1-mmol K_2CO_3, and 2-propanol/H_2O mixture (1:2, v/v) at room temperature.

The optimization reaction condition on hand, the Suzuki–Miyaura cross-coupling reaction of different aryl bromides with various phenylboronic acid derivatives, was examined (Table 2). First, the cross-coupling reaction of various electron-withdraw *p*-substituted aryl bromides contains CN, NO_2, $COCH_3$, CH_3, OCH_3, and CF_3 groups with substituted phenylboronic acid such as 4-*tert*-buthylboronic acid, 2-methoxyboronic acid, and 3-formyl-4-methoxybornic acid investigated. The results clearly showed that the reaction could be completed in 0.3–5 min with excellent yields for electron-withdrawing substituted aryl bromides and substituted phenylboronic acids. The Suzuki cross-coupling reaction of electron-donating aryl bromides with substituted phenylboronic acids takes a longer time for high yields. Besides, the cross-coupling reaction of *o*-substituted aryl bromides with boronic acid derivatives needs more reaction time due to the substituted group's steric hindrance. The cross-coupling reaction of 5-bromofuraldehyde was also tested, and the result was satisfactory (Table 2, Entry 10). In the coupling reaction of 2,6-dibromopyridine, mono or diarylated products were obtained with high or moderate selectivity, depending on the type of phenylboronic acid used (Table 2, Entries 12, 34, 41, and 47). The cross-coupling reactions of heteroaryl compounds can be important for different applications such as biological and doing more chemistry.

TABLE 2 Suzuki–Miyaura cross-coupling reactions catalyzed by Magnetite@MCM-41@NHC@Pd catalyst

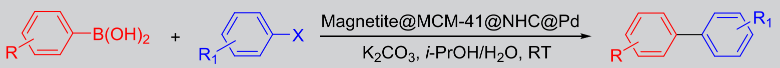

Entry	Ar–B (OH)$_2$	Ar–Br	Product	Time (min)	Yield (%)[a]	TON/TOF/ (h^{-1})
1	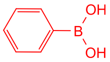	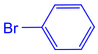	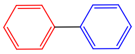	15	100	2217/8867
2		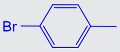	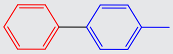	15	98	2230/8740
3		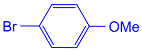	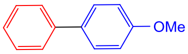	15	94	2229/8379
4		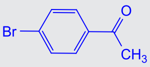	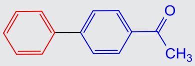	0.3	100	2228/405056
5		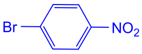	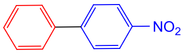	0.3	100	2195/399040
6		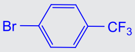	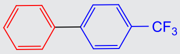	0.3	100	2246/408404
7		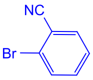	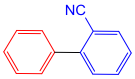	5	95	2192/24992
8		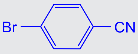	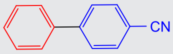	1	100	2192/131538
9		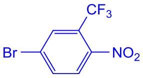	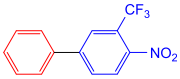	0.3	100	2333/406016

TABLE 2 (Continued)

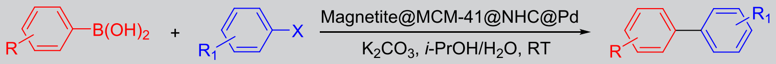

Entry	Ar–B (OH)$_2$	Ar–Br	Product	Time (min)	Yield (%)[a]	TON/TOF/ (h^{-1})
10		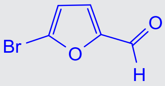	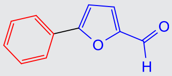	1	100	2229/133760
11		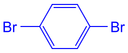	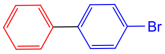	1	32	2254/131197
			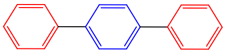		65	
12		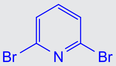	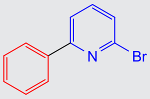	15	100	2245/6734
13	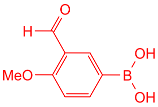	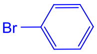	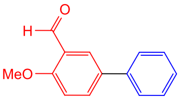	60	79	2217/1751
14		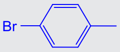	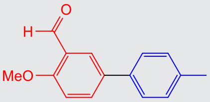	60	73	2230/1627
15		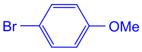	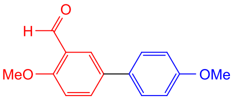	60	59	2229/1315
16		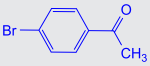	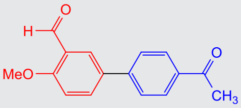	1	100	2228/133668

(Continues)

TABLE 2 (Continued)

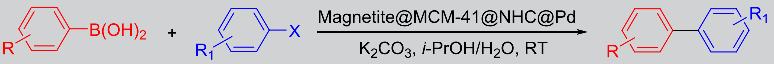

Entry	Ar–B (OH)$_2$	Ar–Br	Product	Time (min)	Yield (%)[a]	TON/TOF/ (h^{-1})
17		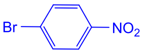	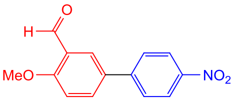	1	100	2195/131683
18		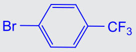	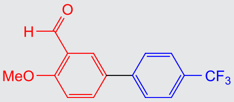	1	100	2246/134773
19		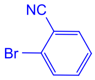	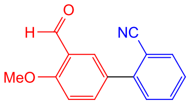	3	94	2192/41215
20		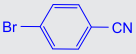	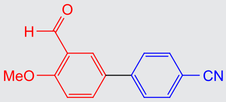	1	100	2192/131538
21		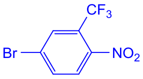	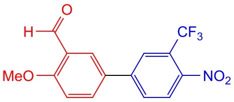	1	100	2233/133985
22		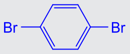	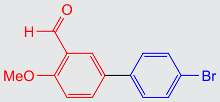	3	66	2254/29756
23	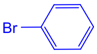	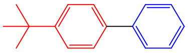	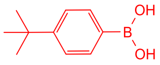	10	94	2217/12502
24		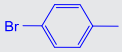	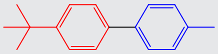	10	100	2230/13378

TABLE 2 (Continued)

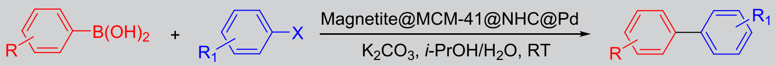

Entry	Ar–B (OH)$_2$	Ar–Br	Product	Time (min)	Yield (%)[a]	TON/TOF/ (h^{-1})
25		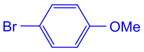	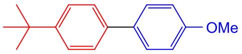	10	97	2229/12970
26		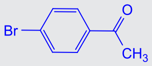	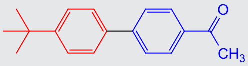	0.3	100	2228/405056
27		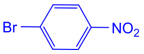	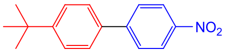	0.3	100	2195/399040
28		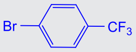	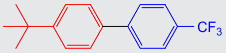	0.3	100	2246/408404
29		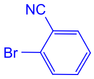	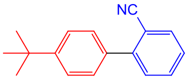	2	100	2192/65769
30		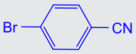	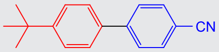	0.3	100	2192/398601
31		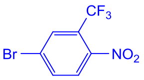	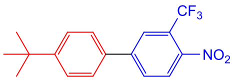	0.3	100	2233/406016
32		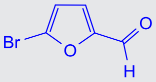	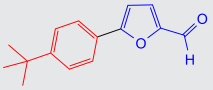	1	100	2229/133760
33		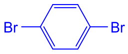	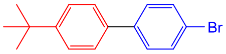	1	38	2254/135254

(Continues)

TABLE 2 (Continued)

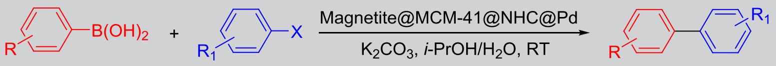

Entry	Ar–B (OH)$_2$	Ar–Br	Product	Time (min)	Yield (%)[a]	TON/TOF/ (h^{-1})
			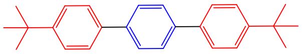		62	
34		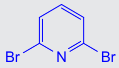	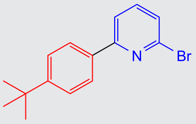 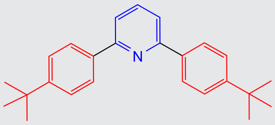	15	65 35	2245/8979
35	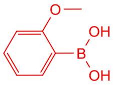	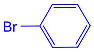	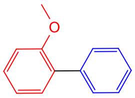	20	94	2217/6251
36		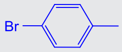	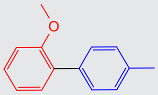	20	100	2230/6689
37		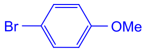	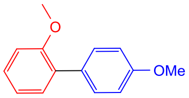	20	100	2229/6686
38		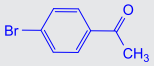	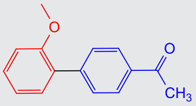	2	100	2228/66834
39		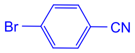		2	100	2192/65769

TABLE 2 (Continued)

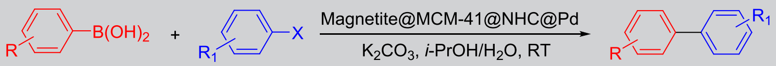

Entry	Ar–B (OH)$_2$	Ar–Br	Product	Time (min)	Yield (%)[a]	TON/TOF/ (h^{-1})
			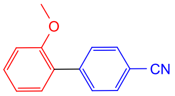			
40		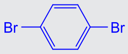	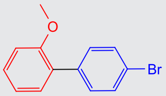	1	9	2254/135254
			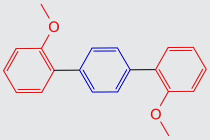		91	
41		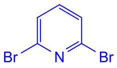	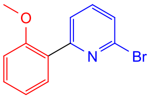	15	75	2245/8979
			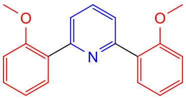		25	
42	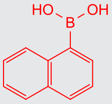	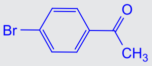	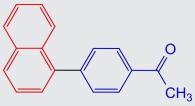	1	100	2228/133668
43		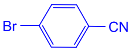	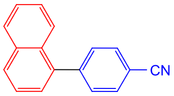	1	100	2192/131538

(Continues)

TABLE 2 (Continued)

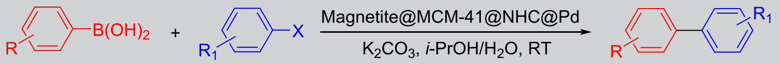

Entry	Ar–B (OH)$_2$	Ar–Br	Product	Time (min)	Yield (%)[a]	TON/TOF/ (h^{-1})
44		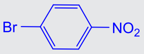	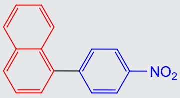	1	100	2195/131683
45		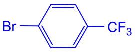	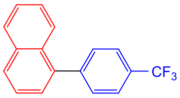	1	100	2246/134773
46		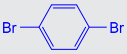	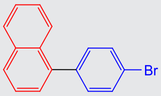	3	62	2254/45084
			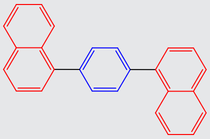		38	
47		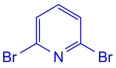	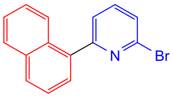	15	54	2245/7991
			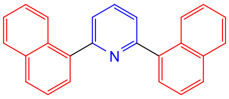		35	

[a] Reaction conditions: Magnetite@MCM-41@NHC@Pd (0.01127 mmol% Pd), phenylboronic acid (0.6 mmol), aryl bromide (0.5 mmol), base (1.0 mmol), *i*-PrOH/water (1:2, 3 ml), room temperature. Gas chromatography (GC) yields determine according to aryl bromide using (trifluoromethyl)benzene as an internal standard.

The reusability of the catalyst was examined in the coupling of 4-bromoacetophenone with PhB (OH)$_2$. The results from reusing this catalyst are shown in Figure 9. For this purpose, after each reaction, the catalyst was removed from reaction media by a magnet and prepared for the next run by washing with 2-propanol and water and dried at 80°C for 3 h. The results show that the Magnetite@MCM-41@NHC@Pd catalyst can be used up to 10 times without a significant decrease in its catalytic performance.

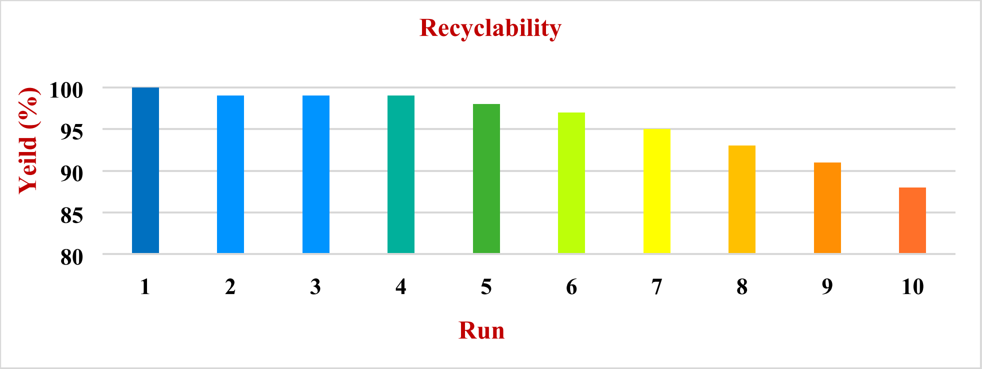

FIGURE 9 Recyclability of the Magnetite@MCM-41@NHC@Pd catalyst for the Suzuki–Miyaura cross-coupling reaction

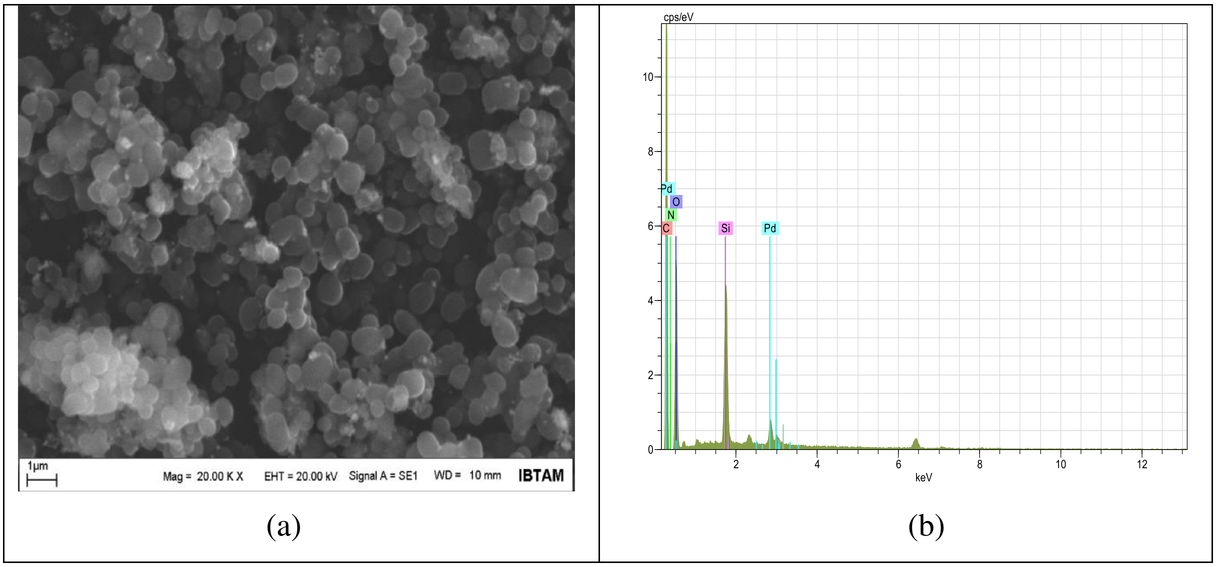

FIGURE 10 (a) The scanning electron microscopy (SEM) image and (b) energy disperse X-ray analysis (EDX) spectra of 10 times used catalyst

A filtration test was performed at room temperature to understand whether the palladium is leaching from the catalyst structure while performing the reaction. For this aim, we used 4-methoxybenzene with phenylboronic acid. Five minutes after starting the reaction, the catalyst was removed from the reaction medium by a magnet. Meanwhile, the sample taken from the reaction medium analyzes by GC. The rest solution, with no catalyst, was stirred for a further 5 min at room temperature. After 5 min, the sample for GC analysis was taken. According to the GC results, the yield was observed the same after the 5th and 10th minutes. It concludes that the Pd metal did not leach out, and the catalyst seems to be very stable under these reaction conditions. To validate the room temperature filtration test, the Pd amount in the 10 times used catalyst was determined by ICP-OES analysis and found a value very close to the initial amount (0.589 wt% Pd), which indicated that the leaching of Pd from the support material is very limited and thus not affect to catalyst performance significantly. For this reason, the reused catalyst can catalyze 10 times Suzuki reactions without substantially losing performance. The strong sigma NHC ligand bond with the Pd metal plays a vital role in preventing Pd leaching from the support material. As it is known, NHCs show powerful sigma donor properties than many known famous ligands such as phosphines and pyridine. These are some of the prime properties in both heterogeneous catalysis and homogeneous catalysis.

3.2 | Characterization of the recovered catalyst

The SEM and EDX analysis were used to investigate the changes in the catalyst structure and stability. The SEM and EDX results show minimal structural changes and agglomeration on the catalyst structure (Figure 10). The slight decrease in the catalytic performance of the catalyst supports these data.

3.2.1 | Poisoning test

The poisoning tests were performed using polyvinylpyrrolidone (PVP) and mercury to determine the homogeneity/heterogeneity nature of catalysis described here.[74–76] As shown in Scheme 1, palladium immobilized on the surface of Magnetite@MCM-41@NHC@Pd by a covalent bond. If the Pd metal leaches from the catalyst structure and takes place in the reaction solution, both heterogeneous (supported) and homogeneous (leached) palladium catalyze the reaction as a catalyst. However, the homogeneous catalyst activity can be stopped by adding ligands, which insoluble in the reaction medium, that can bind palladium. Commercially available PVP often uses for this purpose. Herein, the PVP ligand was used in the poisoning test. Addition of the PVP ligand to the Suzuki–Miyaura reaction of 4-bromoacetophenon with PhB $(OH)_2$ did not prevent product formation. The obtained yield was 100%, and it should be due to the heterogeneous nature of the Magnetite@MCM-41@NHC@Pd.

After these catalytic reactions, our Magnetite@MCM-41@NHC@Pd catalyst has shown fanciful catalytic activity on the Suzuki–Miyaura reaction of various boronic acids and different aryl bromides. Comparing the activities of our catalyst with similar types of magnetic or nonmagnetic heterogeneous palladium catalysts in Suzuki reactions,[37,39,77–85] it shows that the catalyst in this study has better catalytic activity and applications than many reported similar catalysts (Table 3). In the literature,[37,39,77–85] the most of the Suzuki–Miyaura cross-coupling reactions catalyzed by similar types of catalysts require high temperatures for coupled product formation. However, in our catalytic system, similar products were easily synthesized at room temperature with high yields and very high turnover frequency (TOF) values. Furthermore, it is seen that the amount of catalyst loadings in the literature is considerably higher than our catalytic system. As far as we know, the amount of catalyst loading at our system has the lowest value for the Suzuki cross-coupling system. Although our catalytic system positively differentiated from reported

TABLE 3 Comparison of Magnetite@MCM-41@NHC@Pd in the Suzuki–Miyaura reaction of 4-bromobenzonitrile with phenylboronic acid with reported catalysts

Reference	Cat. (mol%), solvent, temperature	Time (min)	Yield (%)
Ghorbani-Choghamarani et al.[76]	CMC-NHC-Pd (0.8 mol%), EtOH/H_2O (1:1), 60°C, X = Br, X^a = Cl	180, 300^a	94, 52^a
Karimi and Akhavan[77]	γ-Fe_2O_3-acetamidine-Pd, DMF, 100°C, X = Br	120, 30^b	92, 96^b
Ke te al.[78]	Cell-NHC-Pd (0.75 mol%), DMF/H_2O (1:1), 80°C, X = Br	120	99
Khajehzadeh and Moghadam[79]	Pd/C-NHC-P $(OR)_3$ (0.03 mol%), EtOH, 80°C, X = Br	60	98
Esmaeilpour et al.[39]	Fe_3O_4@SiO_2@VB1-Pd NPs (0.022 mol%), EtOH, 60°C, X = Br	20, 20^b	98, 95^b
Dhameliya et al.[37]	Fe_3O_4@SiO_2-NHC-$Pd^{(II)}$ (0.37 mol%), H_2O, 60°C, X = I	60, 90^b	92, 93^b
Khazaei et al.[80]	Pd-TEG, (0.005 mol%) H_2O, 25°C, X = Br	840	91
Le et al.[81]	$(Pd^{II}\text{-NHC})_n$@SiO_2 (0.27 mol%), DMF/H_2O (2:1), 60°C, X = Br	8^b	95^b
Singha Roy et al.[82]	SBA-15/CCPy/Pd (II) (0.3 mol%), EtOH/H_2O (2:1), 50°C, X = I	60	98
Sobhani et al.[83]	Fe_3O_4@SiO_2@mSiO_2-Pd (II)(0.5 mol%), EtOH, 80°C, X = Br	480^b	95^b
Veisi et al.[84]	Fe_3O_4@SiO_2-Pd (II)(0.03 mol%), EtOH, 85°C, X = Br	65,30^b	85, 90^b
This work	Fe_3O_4@MCM-41@NHC@Pd (0.01127 mmol%, *i*-PrOH/H_2O (1:2), rt, X = Br	1, 15^b	100, 100^b

[a]Yield obtained for 4-chlorobenzene substrate.

[b]Yield obtained for 4-bromobenzene substrate.

catalytic systems,[35,37,77–85] the disadvantage of the catalytic system in this study is ineffective with aryl chloride substrates at room temperature. Consequently, our catalyst showed extraordinary catalytic activity when considering the reaction parameters such as catalyst loading, high efficiency with aryl bromides, and reaction temperature. It may be a potential catalyst for other organic transformations due to encouraging catalytic results.

4 | CONCLUSIONS

An efficient and green Magnetite@MCM-41@NHC@Pd catalyst was synthesized and applied for Suzuki–Miyaura reaction to synthesize fine substituted and biologically important biaryls. This novel catalyst shows excellent catalytic activity (turnover number [TON] = 2246 and TOF 408404 h^{-1}) with high reusability in Suzuki–Miyaura reactions. This catalyst has high strong magnetic and dispersing properties. These properties help increase catalytic activity and recovery of catalyst from reaction media. Stability toward the air, moisture, low loading, easy handling, and recyclability is the unique features of our catalyst. The applicability of this catalyst in other palladium-catalyzed catalytic systems is under research in our lab. We expect that it will provide high catalytic activity with reusability in different reactions.

ACKNOWLEDGMENTS

XPS and TEM studies were performed in France (CEA LETI/DTSI/SCMC Grenoble Cedex 9 FRANCE and thanks to N. GAMBACORTI for organization of XPS and TEM analysis) within the framework of the NFFA-Europe Transnational Access Activity (NFFA Project ID: 723).

AUTHOR CONTRIBUTIONS

Mitat Akkoç: Formal analysis; investigation; methodology; project administration; resources. **Nesrin Buğday:** Formal analysis; investigation; methodology; project administration; resources. **serdar altın:** Formal analysis; investigation; resources. **Sedat Yasar:** Formal analysis; funding acquisition; investigation; methodology; project administration; resources; supervision.

DATA AVAILABILITY STATEMENT

The data that support the findings of this study are openly available in the supporting information of this article.

CONFLICT OF INTERESTS

The authors declare that they have no known competing financial interests or personal relationships that could have appeared to influence the work reported in this paper.

ORCID

Mitat Akkoç https://orcid.org/0000-0001-8641-8958
Nesrin Buğday https://orcid.org/0000-0002-3882-035X
Serdar Altın https://orcid.org/0000-0002-4590-907X
Sedat Yaşar https://orcid.org/0000-0001-7285-2761

REFERENCES

[1] A. Ghorbani-Choghamarani, P. Moradi, B. Tahmasbi, *J. Iran. Chem. Soc.* **2019**, *16*, 511.
[2] A. Ghorbani-Choghamarani, M. Nikoorazm, H. Goudarziafshar, B. Tahmasbi, *Bull. Korean Chem. Soc.* **2009**, *30*, 1388.
[3] H. Hassani, B. Zakerinasab, A. Nozarie, *Asian J. Green Chem.* **2018**, *3*, 59.
[4] P. Ju, S. Wu, Q. Su, X. Li, Z. Liu, G. Li, Q. Wu, *J. Mater. Chem. A* **2019**, *7*, 2660.
[5] R. R. Langeslay, D. M. Kaphan, C. L. Marshall, P. C. Stair, A. P. Sattelberge, M. Delferro, *Chem. Rev.* **2019**, *119*, 2128.
[6] Y. Rangraz, F. Nemati, A. Elhampour, *New J. Chem.* **2018**, *42*, 15361.
[7] (a)M. Zarei, H. Sepehrmansourie, M. A. Zolfigol, R. Karamian, S. H. Moazzami Farida, *New J. Chem.* **2018**, *42*, 14308. (b)S. Moradi, M. A. Zolfigol, M. Zarei, D. A. Alonso, A. Khoshnood, A. Tajally, *Appl. Organomet. Chem.* **2018**, *32*, 4043.
[8] M. Bahadori, S. Tangestaninejad, M. Moghadam, V. Mirkhani, A. Mechler, I. Mohammadpoor-Baltork, F. Zadehahmadi, *Microporous Mesoporous Mater.* **2017**, *253*, 102.
[9] A. Fihri, M. Bouhrara, B. Nekoueishahraki, J. M. Basset, V. Polshettiwar, *Chem. Soc. Rev.* **2011**, *40*, 5181.
[10] M. Gholinejad, Z. Naghshbandi, C. Nájera, *ChemCatChem* **2019**, *11*, 1792.
[11] M. Ghotbinejad, A. R. Khosropour, I. Mohammadpoor-Baltork, M. Moghadam, S. Tangestaninejad, V. Mirkhani, *J. Mol. Catal. A: Chem.* **2014**, *385*, 78.
[12] S. Hemmati, L. Mehrazin, M. Pirhayati, H. Veisi, *Polyhedron* **2019**, *158*, 414.
[13] G. Mohammadi Ziarani, S. Rohani, A. Ziarati, A. Badiei, *RSC Adv.* **2018**, *8*, 41048.
[14] Y. Chen, H. R. Chen, L. M. Guo, Q. J. He, F. Chen, J. Zhou, J. Feng, J. Shi, *ACS Nano* **2010**, *4*, 529.
[15] M. Esmaeilpour, J. Javidi, *J. Chin. Chem. Soc.* **2015**, *62*, 614.
[16] H. Firouzabadi, N. Iranpoor, M. Gholinejad, J. Hoseini, *Adv. Synth. Catal.* **2011**, *353*, 125.
[17] A. A. Jafari, H. Mahmoudi, H. Firouzabadi, *RSC Adv.* **2015**, *5*, 107474.
[18] D. Shi, H. S. Cho, Y. Chen, H. Xu, H. Gu, J. Lian, W. Wang, G. Liu, C. Huth, L. Wang, R. C. Ewing, S. Budko, G. M. Pauletti, Z. Dong, *Adv. Mater.* **2015**, *21*, 2170.
[19] H. Zhang, X. Zhong, J. J. Xu, H. Y. Chen, *Langmuir* **2008**, *24*, 13748.
[20] S. J. Zhang, X. H. Liu, L. P. Zhou, W. J. Peng, *Mater. Lett.* **2012**, *68*, 243.
[21] K. Mal, S. Chatterjee, A. Bhaumik, C. Mukhopadhyay, *ChemistrySelect* **2019**, *4*, 1776.

[22] M. Nikoorazm, A. Ghorbani Choghamarani, A. Panahi, B. Tahmasbi, N. Noori, *J. Iran. Chem. Soc.* **2018**, *15*, 181.

[23] M. Nikoorazm, A. Ghorbani-Choghamarani, N. Noori, B. Tahmasbi, *Appl. Organomet. Chem.* **2016**, *30*, 843.

[24] S. You, R. Xiao, H. Liu, M. Cai, *New J. Chem.* **2017**, *41*, 13862.

[25] M. G. Adimoolam, N. Amreddy, M. Rao Nalam, M. V. Sunkara, *J. Magn. Magn. Mater.* **2018**, *448*, 199.

[26] M. S. Ghasemzadeh, B. Akhlaghinia, *New J. Chem.* **2019**, *43*, 5341.

[27] A. Ghorbani-Choghamarani, B. Tahmasbi, N. Noori, R. Ghafouri-Nejad, *J. Iran. Chem. Soc.* **2017**, *14*, 681.

[28] H. Mohamadi Tanuraghaj, M. Farahi, *New J. Chem.* **2019**, *43*, 4823.

[29] M. S. Saeedi, S. Tangestaninejad, M. Moghadam, V. Mirkhani, I. Mohammadpoor-Baltork, A. R. Khosropour, *Polyhedron* **2013**, *49*, 158.

[30] F. Shi, H. Shan, D. Li, X. Yin, J. Yu, B. Ding, *J. Colloid Interface Sci.* **2019**, *538*, 620.

[31] L. Shiri, B. Tahmasbi, *Phosphorus, Sulfur Silicon Relat. Elem.* **2017**, *192*, 53.

[32] M. Tadic, S. Kralj, Y. Lalatonne, L. Motte, *Appl. Surf. Sci.* **2019**, *476*, 641.

[33] M. Nikoorazm, F. Ghorbani, A. Ghorbani-Choghamarani, Z. Erfani, *Chin. J. Catal.* **2017**, *38*, 1413.

[34] B. Tahmasbi, A. Ghorbani-Choghamarani, *New J. Chem.* **2019**, *43*, 14485.

[35] K. V. S. Ranganath, J. Kloesges, A. Schfer, F. Glorius, *Am. Ethnol.* **2010**, *122*, 7952.

[36] P. D. Stevens, G. Li, J. Fan, M. Yen, Y. Gao, *Chem. Commun.* **2005**, *35*, 4435.

[37] T. M. Dhameliya, H. A. Donga, P. V. Vaghela, B. G. Panchal, D. K. Sureja, K. B. Bodiwala, M. T. Chhabria, *RSC Adv.* **2020**, *10*, 32740.

[38] H. A. Elazabb, A. R. Siamaki, S. Moussaa, B. F. Guptona, M. S. El-Shall, *Appl. Catal., A* **2015**, *491*, 58.

[39] M. Esmaeilpour, A. R. Sardarian, H. Firouzabadi, *J. Organomet. Chem.* **2018**, *873*, 22.

[40] M. Gholinejad, M. Razeghi, C. Najera, *RSC Adv.* **2015**, *5*, 49568.

[41] A. Ghorbani-Choghamarani, G. Azadi, *Appl. Organomet. Chem.* **2016**, *30*, 247.

[42] B. Karimi, F. Mansouri, H. Vali, *Green Chem.* **2014**, *16*, 2587.

[43] H. Liu, P. Wang, H. Yang, J. Niu, J. Ma, *New J. Chem.* **2015**, *39*, 4343.

[44] A. Nuri, Y. Mansoori, A. Bezaatpour, A. Shchukarev, J. P. Mikkola, *ChemistrySelect* **2019**, *4*, 1820.

[45] F. Rafiee, S. A. Hosseini, *Appl. Organomet. Chem.* **2018**, *4519*.

[46] F. Rafiee, N. Mehdizadeh, *Catal. Lett.* **2018**, *148*, 1345.

[47] K. V. S. Ranganath, A. H. Schfer, F. Glorius, *ChemCatChem* **2011**, *3*, 1889.

[48] W. Tang, J. Li, X. Jin, J. Sun, J. Huang, R. Li, *Catal. Commun.* **2014**, *43*, 75.

[49] Z. Vargas-Osorio, M. A. Gonzalez-Gomez, Y. Pineiro, C. Vazquez-Vazquez, C. Rodrıguez-Abreu, M. A. Lopez-Quintela, J. Rivas, *J. Mater. Chem. B* **2017**, *5*, 9395.

[50] H. Veisi, M. Hameliana, S. Hemmati, *J. Mol. Catal. A Chem.* **2014**, *395*, 25.

[51] D. Wang, W. Liu, F. Bian, W. Yu, *New J. Chem.* **2015**, *39*, 2052.

[52] F. Zhang, M. Chen, X. Wu, W. Wang, H. Li, *J. Mater. Chem.* **2014**, *2*, 484.

[53] Y. Zheng, P. D. Stevens, Y. Gao, *J. Org. Chem.* **2006**, *71*, 537.

[54] Y. Liu, X. Bai, S. Li, *Microporous Mesoporous Mater.* **2018**, *260*, 40.

[55] H. Matsumoto, T. Akiyoshi, Y. Hoshino, H. Seto, Y. Miura, *Polym. J.* **2018**, *50*, 1179.

[56] A. M. Trzeciak, A. W. Augustyniak, *Coord. Chem. Rev.* **2019**, *384*, 1.

[57] aŞ. Yaşar, T. K. Köprülü, Ş. Tekin, S. Yaşar, *Inorg. Chim. Acta* **2018**, *479*, 17. bŞ. Yaşar, T. K. Köprülü, Ş. Tekin, S. Yaşar, *Appl. Organomet. Chem.* **2018**, *32*, 4016. cM. Akkoç, S. Balcıoğlu, C. Gürses, T. T. Tok, B. Ateş, S. Yaşar, *J. Organomet. Chem.* **2018**, *869*, 67.

[58] X. Liu, Z. Ma, J. Xing, H. Liu, *J. Magn. Magn. Mater.* **2004**, *270*, 1.

[59] A. Ghorbani-Choghamarani, B. Tahmasbi, R. H. E. Hudson, A. Heidari, *Microporous Mesoporous Mater.* **2019**, *284*, 366.

[60] A. Ghorbani-Choghamarani, B. Tahmasbi, N. Noori, S. Faryadi, *C. R. Chim.* **2017**, *20*, 132.

[61] M. Nikoorazm, N. Noori, B. Tahmasbi, S. Faryadi, *Transition Met. Chem.* **2017**, *42*, 469.

[62] A. Ghorbani-Choghamarani, M. Hajjami, B. Tahmasbi, N. Noori, *J. Iran Chem. Soc.* **2016**, *13*, 2193.

[63] V. Kandathil, B. D. Fahlman, B. S. Sasidhar, S. A. Patild, S. A. Patil, *New J. Chem.* **2017**, *41*, 9531.

[64] Y. Huang, J. Tang, L. Gai, Y. Gong, H. Guang, R. He, H. Lyu, *Chem. Eng. J.* **2017**, *319*, 229.

[65] X. Wang, H. Pan, Q. Lin, H. Wu, S. Jia, Y. Shi, *Nanoscale Res. Lett.* **2009**, *14*, 259.

[66] A. M. A. Imad, A. M. Barbara, *PNAS* **2008**, *18*, 1736.

[67] F. Heidari, M. Hekmati, H. Veisi, *J. Colloid Interface Sci.* **2017**, *501*, 175.

[68] M. Sabo, A. Henschel, H. Fröde, E. Klemmb, S. Kaskel, *J. Mater. Chem.* **2007**, *17*, 3827.

[69] R. Aghaei, A. Eshaghi, *J. Alloys Compd.* **2017**, *699*, 112.

[70] A. Ghorbani-Choghamarani, P. Moradi, B. Tahmasbi, *RSC Adv.* **2016**, *6*, 56458.

[71] aZ. I. Dehimat, S. Yaşar, D. Tebbani, I. Ozdemir, *Inorg. Chim. Acta* **2018**, *469*, 325. bS. Yaşar, M. Akkoç, N. Ozdemir, I. Ozdemir, *Turk. J. Chem.* **2019**, *43*, 1622. cM. Akkoç, F. İmik, V. Dorcet, T. Roisnel, C. Bruneau, I. Ozdemir, *ChemistrySelect* **2017**, *2*, 5729. d E. O. Karaca, M. Akkoç, S. Yaşar, I. Ozdemir, *ARKIVOC* **2018**, *part v.* 0 eE. O. Karaca, M. Akkoç, M. N. Tahir, C. Arıcı, F. Imik, N. Gürbüz, S. Yaşar, I. Ozdemir, *Tetrahedron Lett.* **2017**, *58*, 3529.

[72] aF. Imik, S. Yaşar, I. Ozdemir, *J. Organomet. Chem.* **2009**, *896*, 162. bF. Imik, S. Yaşar, I. Ozdemir, *Inorg. Chim. Acta* **2019**, *495*, 118969.

[73] aN. Touj, N. Gürbüz, N. Hamdi, S. Yasar, I. Ozdemir, *Inorg. Chim. Acta* **2018**, *478*, 187. bN. Touj, S. Yasar, N. Ozdemir, N. Hamdi, I. Ozdemir, *J. Organomet. Chem.* **2018**, *860*, 59.

[74] T. Baran, E. Acıksöz, A. Mentes, *J. Mol. Catal. A: Chem.* **2015**, *407*, 47.

[75] Y. Dong, X. Wu, X. Chen, Y. Wei, *Carbohydr. Polym.* **2017**, *160*, 106.

[76] A. Ghorbani-Choghamarani, P. Moradi, B. Tahmasbi, *Polyhedron* **2019**, *163*, 98.

[77] B. Karimi, P. F. Akhavan, *Chem. Commun.* **2011**, *47*, 7686.

[78] H. Ke, X. Chen, G. Zou, *Appl. Organomet. Chem.* **2014**, *28*, 54.

[79] M. Khajehzadeh, M. Moghadam, *J. Organomet. Chem.* **2018**, *863*, 60.

[80] A. Khazaei, M. Khazaei, M. Nasrollahzadeh, *Tetrahedron* **2017**, *73*, 5624.

[81] X. Le, Z. Dong, Z. Jin, Q. Wang, J. Ma, *Catal. Commun.* **2014**, *53*, 47.

[82] A. Singha Roy, J. Mondal, B. Banerjee, P. Mondal, A. Bhaumik, S. Manirul Islam, *Appl. Catal. A. Gen.* **2014**, *469*, 320.

[83] S. Sobhani, M. S. Ghasemzadeh, M. Honarmand, F. Zarifi, *RSC Adv.* **2014**, *4*, 44166.

[84] H. Veisi, M. Hamelian, S. Hemmati, *J. Mol. Catal. A Chem.* **2014**, *395*, 25.

[85] X. Wang, P. Hu, F. Xue, Y. Wei, *Carbohydr. Polym.* **2014**, *114*, 476.

SUPPORTING INFORMATION

Additional supporting information may be found online in the Supporting Information section at the end of this article.

How to cite this article: Akkoç M, Buğday N, Altın S, Yaşar S. Magnetite@MCM-41 nanoparticles as support material for Pd-*N*-heterocyclic carbene complex: A magnetically separable catalyst for Suzuki–Miyaura reaction. *Appl Organomet Chem*. 2021;e6233. https://doi.org/10.1002/aoc.6233